DUAL SECRETORY VESICLES CLUSTERING AND DYNAMICS DURING POLAR CELL ELONGATION IN THE PHYTOPATHOGENIC FUNGUS *BOTRYTIS CINEREA*

Adrien Hamandjian[1,2], Glen Calvar[1,2], Matthieu Blandenet[1,2], Mélanie Crumière[1,2], Nathalie Poussereau[1,2], Mathias Choquer[1,2#] and Christophe Bruel[1,2#*]

[1]Université Lyon 1, Univ Lyon, CNRS, INSA-Lyon, Bayer, UMR5240 MAP Microbiologie, Adaptation et Pathogénie, 10 Rue Raphaël Dubois, Villeurbanne, F-69622, France.

[2]Bayer SAS, CropScience Division, Laboratoire Mixte, 14 Impasse Pierre Baizet, Lyon, F-69263, France.

* Correspondence: Christophe Bruel – christophe.bruel@univ-lyon1.fr

# These authors contributed equally

SUMMARY

Filamentous fungi grow through a process of polar elongation that is supported by secretory vesicles. These vesicles provide lipids to extend the plasma membrane and, among others, enzymes to synthesize the cell wall. We used confocal microscopy to locate and analyze the dynamics of secretory vesicles transporting a fluorescent chitin synthase CHSIIIa in the plant pathogen *Botrytis cinerea*. Two populations of growing hyphae were identified, one exhibiting a typical spheroidal spitzenkörper at the apex, the other one with vesicles forming a crescent instead. Neither curvature of the apex nor hyphal width significantly differ between the two populations. Mean hyphal elongation was also no different between the two populations, with two co-existing patterns of pronounced and less pronounced stepwise extensions. In contrast the growing spitzenkörper-hyphae displayed repetitive fluctuations in fluorescence intensity at the apex that were not detected in the crescent-hyphae. Using Fast Fourier Transform, these fluctuations were found periodic, and a single oscillator was determined that could explain the experimental data.

Introduction

Sustained polar cell elongation is a shared trait in various branches of the tree of life, from the growth of filamentous bacteria and actinomycetes to the morphogenesis of neurons in animals (Boutillon et al., 2024; Takano et al., 2019). In plants, it supports the development of pollen tubes, root hairs, and mosses protonemata (Geitmann, 2010; Carol and Dolan, 2002; M Braun & C Limbach, 2006; Domozych et al., 2013). In eukaryotic microorganisms, polar cell elongation has been described in green algae (Braun et al., 1999; Braun et al., 2004) and in yeasts such as *Candida albicans* and *Ashbya gossypii*, whose respective pathogeny to human and cotton relies on the production of filaments (Crampin et al., 2005; Köhli et al., 2008). More notably, it is a

hallmark of the vegetative growth of filamentous fungi and oomycetes. Understanding polar cell elongation is therefore of general interest. In fungi it is moreover of interest to agriculture and medicine for the search of new solutions to fight pathogenic species, and in biotechnology where filamentous fungi are essential microorganisms, from their use in biopolymer making to the production of commercial enzymes (Cairns et al., 2021; Jadhav et al., 2024).

Polarized cell elongation in fungi relies on the continuous production of secretory vesicles (SVs) by the Golgi apparatus. These vesicles carry membrane proteins, notably cell wall biosynthetic enzymes, and soluble proteins to be delivered to the extracellular environment. These soluble proteins include lytic enzymes, required for nutrition by absorbotrophy, and virulence factors in the case of pathogenic species. SVs are transported to the cell tip by microtubules and/or actin cables. There, they fuse to the plasma membrane, incorporating their lipids content and delivering the cell wall biosynthetic enzymes required for cell wall extension.

Just behind the hyphal tip, a dense cluster of vesicles inter-wined with actin filaments has been described in several fungal species and is acknowledged as a fungal-specific structure called the Spitzenkörper (Spk) (Harris et al., 2005; Virag and Harris, 2006; Steinberg, 2007; Riquelme, 2013; Riquelme and Sanchez-Leon, 2014; Zhou et al., 2018). This Spk was reported in growing hyphae and it is proposed as a vesicle supply center for apical elongation (Bartnicki-Garcia et al., 1989; Löpez-Franco and Bracker, 1996; Gierz and Bartnicki-Garcia, 2001; Köhli et al., 2008). It can be disrupted upon perturbation of actin polymerization (Crampin et al., 2005; Taheri-Talesh et al., 2008; Jones and Sudbery, 2010) or in mutants affected in the fusion of SV to the plasma membrane (Bernardo et al., 2014).

The current model of SV fusion to the plasma membrane involves calcium and two main multi-protein complexes named the polarisome (Jones and Sudbery. 2010; Xie and Miao, 2021) and the exocyst (Jones and Sudbery, 2010; Riquelme et al. 2014). In this model, the polarisome controls the nucleation of actin at the hyphal tip. The resulting actin filaments, formed in the retrograde direction, produces a scaffold that hinders the contact between the vesicles and the plasma membrane. Upon calcium influx, actin depolymerizes and the exocyst tethers the SVs before SNARE-mediated fusion with the plasma membrane. Reseting the calcium level to its initial value allows the system to cycle. This oscillatory model is supported by the observation of exocytic bursts at the apex of *Neurospora crassa* hyphae (Riquelme et al., 2014) and by the oscillating intensities of fluorescent markers of actin and SVs at the apex of *A. nidulans* and *N. crassa* hyphae (Ishitsuka et al., 2015; Takeshita et al., 2017). In line with this model, the Spk could originate from the accumulation of SVs at the apex when their fusion with the plasma membrane is limited,

relatively to their supply by the Golgi apparatus. Besides, this model predicts periodic accumulations of SVs at the apex, leading to a stepwise cell elongation each time exocytosis takes place.

To our knowledge, the oscillatory dynamic of tip growth in filamentous fungi has been investigated once (Takeshita et al. 2017). This pioneer study in the saprophytic ascomycetes *A. nidulans* and *N. crassa* used live-cell imaging analysis to reveal the calcium-dependent dynamics of SVs and actin mentioned above. Here we used a similar approach to explore tip growth in the plant pathogen *Botrytis cinerea*, the causing agent of grey mold in hundreds of plants (Singh et al. 2024). Whether the dynamics of SVs at the filaments tip is a common process in all growing hyphae was investigated and a pipeline using signal clustering and Fast Fourier Transform was established to detect putative populations with different behaviors. Whether a stepwise pattern of hyphal elongation could be detected in this fungus as in *A. nidulans* or *N. crassa* was also studied.

Material and methods

a) Plasmids and Strains production

The strains BcCHSIIIa::eGFP and eGFP^{Cyt} were obtained by *Agrobacterium tumefaciens* mediated transformation of the *B. cinerea* strain B05-10 (Rolland et al., 2003). The BcCHSIIIa::eGFP strain was generated by the insertion, through homologous recombination, of an eGFP-tNiaD-NatR DNA fragment in frame with the *BcCHSIIIa* (Bcin04g03120) coding sequence. This DNA fragment, containing eGFP optimized for *B. cinerea* (Leroch et al. 2011), the terminator of the nitrate reductase from *B. cinerea* (tNiaD) and a nourseothricine resistance gene (NatR), was amplified from a donor plasmid (unpublished). Using double-joint PCR (Hamari et al. 2004), it was then assembled, at the 5' end, with the last 1031 bp of the *BcCHSIIIa* coding sequence (minus the stop codon) and, at the 3' end, with the 3'UTR plus the terminator region (924 pb) of the *BcCHSIIIa* gene. These flanks were amplified from B05-10 genomic DNA. The resulting DNA cassette was inserted by *In Vivo* Assembly (IVA) cloning into a *A. tumefasciens* transfer-DNA carried by the p7 vector (García-Nafría et al. 2016). Following verification by restriction enzyme digestion and sequencing, the vector was introduced in *A. tumefasciens* (strain LDA 1126) and the transformed bacteria was used to mutagenize *B. cinerea*. In parallel, the eGFP^{Cyt} strain was obtained by ectopic insertion in the fungal genome of a cassette containing eGFP under the control of the OliC promoter from *A. nidulans* (Souibgui et al. 2021) and tNiaD. This cassette was placed in a *A. tumefasciens* transfer-DNA carried by the pBHT2 plasmid containing a hygromycin resistance gene (Mullins et al. 2007). Nourseothricin-resistant (70 µg/ml) and hygromycin-resistant (70 µg/ml) *B. cinerea* transformants were screened by fluorescence microscopy to verify the

101 expected localization of eGFP, and by PCR to verify the presence of the resistance genes, the eGFP
102 gene and the correct fusion of *BcCHSIIIa* and eGFP.

103 b) Image acquisition

104 Images of growing hyphae from *B. cinerea* were acquired after 48 hours of incubation at 21°C in a
105 96-well microplate containing 200 µl MMII medium ($NaNO_3$ 24 mM, Glucose 111 mM, KH_2PO_4
106 0.147 mM, $MgSO_4$ 0.039 mM, KCl 0.134 mM, $FeSO_4/7H_2O$ 0.7 µM) inoculated with 200 conidia
107 from frozen stocks. Time-lapse acquisitions (10 min) were conducted using a laser scanning
108 confocal microscope (ZEISS Observer 7 equipped with an LSM 800) and a Plan-Apochromat 63x
109 Oil DIC objective. Excitation was achieved using a 493 nm laser, and fluorescence emissions were
110 detected within the range of 491 to 573 nm. The laser scanning was performed with an averaging
111 of 16. To ensure a uniform acquisition speed between images, the size of the acquired region was
112 standardized (295x224 pixels) leading to an acquisition rate of 4.456 seconds per frame. To
113 harmonize the time series length, only the 135 first frames of each acquisition were analyzed.

114 c) Image analysis

115 All image analysis were performed using FIJI and Python. To limit the bias induced by extracellular
116 pixels, a 50x50 pixels region of interest (ROI) outside the hyphae was defined. The mean of
117 maximal fluorescence intensities in this ROI was measured at each time point of the time-lapse
118 acquisitions. The obtained value plus twice the associated standard deviation was selected as a
119 threshold. Pixels with a fluorescent signal below this threshold were replaced by NaN values.

120 Then, a FIJI macro was created to track and crop the apex of each hypha to a 50x50 pixel ROI that
121 was considered the apical region (4 µm). After thresholding, the mean pixel intensity of the ROI
122 was measured and subtracted by its associated trend (Savitzky-Golay filtering, window length 10,
123 degree 2 polynomial) for each time point of the time-lapse acquisitions.

124 Kymographs were constructed from the 47 first frames (205 seconds, time between pixels 4,456
125 sec). For each time-lapse acquisition, the curvature of the apex was measured on the first frame
126 using the Kappa plugin in FIJI, with a curve length of 10 µm and by taking the curvature of the most
127 apical point. The hyphal width was calculated on the first frame of each acquisition as the average
128 of three measures performed in the distal part of the apical region (3.3 ± 1.2 µm). To measure the
129 geometry and area of maximal fluorescence intensity at the apex, a time-projection and a 1%
130 highest fluorescence threshold were applied.

131 d) Temporal dynamics clustering

Temporal dynamics clustering (TDC) clusters time series based on signal variations through time (Li et al., 2023). Briefly, absolute first-order differences are computed and used to obtain a cumulative distribution function. The *u* parameter is then computed using acquisition parameters with the formula:

$$u = \frac{(T-1)^{\frac{2}{3}}}{log(log(T-1))}$$

where *T* is the length of time series. The element *u* is dependent of the acquisition parameters but not of the measured variable. It is used to determine the quantile I_q that partitions the cumulative distribution function into elements exhibiting common variations (*main* section) from extreme events (*tail* section):

$$I_q = 1 - \frac{u}{T-1}$$

All first-order difference values bellow quantile I_q form the *main* section, while all first-order difference above I_q form the *tail* section. The mean value of the *main* section (μ_{main}), the associated standard deviation (σ_{main}), and the mean value of the *tail* section (μ_{tail}) are then computed for all time series, summarizing each time series by these three coordinates (μ_{main}, σ_{main}, μ_{tail}). Based on this 3-dimensional dataset, Fuzzy C-means was used to identify clusters. Silhouette scores were computed for a range of clusters spanning from 2 to half the number of acquisitions to determine the most satisfying clustering.

e) Fast Fourier Transform

Detection of periodic dynamics commonly uses the Fast Fourier Transform (FFT), an optimized application of the Fourier Transform to discrete signals (e.g. time series). The FFT states that a signal can be divided into a sum of pure sinusoidal waves defined by their period, amplitude and phase shift. It can thus be used to detect periodic variation in complex biological signals.

To obtain a signal corresponding to the apical fluorescence intensity thought time with limited impact from cytosolic background fluorescence, a 16x16 pixels ROI in the sub-apical region (5 ± 2 µm bellow the hyphal tip) was defined post-acquisition. The mean fluorescence intensity in this ROI was measured for the first 20 frames and added to twice the associated standard deviation to obtain a background-level threshold value. All fluorescence values below this threshold were replaced by a NaN values. The mean fluorescence intensity of the apical region was then measured at each time point. The obtained signal was then pre-processed by subtracting its

associated trend obtained by Savitzky-Golay filtering. A second Savitzky-Golay filtered was used to smooth the signal in combination with a moving average.

To increase the resolution of the FFT, all signals were zero-padded to reach a power of two lengths (16 384 total time points). Following FFT, the amplitude at each given frequency *A* was then computed:

$$Amplitude = 2\frac{\sqrt{real[FFT(A)]^2 + imag[FFT(A)]^2}}{N}$$

with *FFT(A)* the FFT output for the frequency *A*, and *N* the length of the time series before zero-padding. For easier biological interpretation, the results were plotted over periods (sec) instead of frequencies (sec^{-1}), producing amplitude spectra. To satisfy the Nyquist sampling theorem, periods below 9 seconds were not considered. In addition, only periods that could be sampled in at least 4 complete cycles during the time-lapse acquisitions (10 min) were considered, ruling out periods above 150 seconds.

Based on the amplitude spectrum, the period with the highest amplitude was used to create a sinusoidal model such as:

$$\eta_n(t) = \sigma_n \cdot sin\left(\frac{2\pi}{p_n}(t - \phi_n)\right)$$

with σ_n the amplitude and ϕ_n the phase shift associated to the period p_n. The value of ϕ_n was estimated by minimizing the Means Squared Error between the model and experimental data for values of ϕ with an angle from 0 to 360°. The estimation of ϕ_n was performed iteratively for all n.

f) Space

Custom Python program was designed to measure the elongation of fungal cell from time-lapse acquisitions. First, threshold and masks were used to differentiate extracellular regions from the cell at each acquisition time. The masks were then used to outline the cell. The outline was then interpolated using a B-spline and points were positioned evenly along the outline. Euclidean distances were computed between points of the outlines corresponding to the first and last frames of the acquisition, the longest distance defining the elongation axis. At each time point, the outline point closest to the elongation axis was determined and projected onto the elongation axis. The distance travelled along the elongation axis between frames was computed for all time points of the acquisition. Because measures are performed at the pixel level after interpolation, retrograde movements were not considered. The linear elongation model corresponds to the elongation axis.

g) Statistics

Statistical analyses were conducted using Python.

Results

Fluorescent chitin synthase IIIa localizes at the tip of growing filaments

To visualize vesicular trafficking at the apex of *B. cinerea* hyphae, a reporter system was required. Based on the successful labelling of SVs through the fluorescent tagging of class III chitin synthases in different ascomycetes (Wernet et al., 2023; Fukuda et al., 2009; Sánchez-León et al., 2011; Zhou et al., 2018), the *B. cinerea* homologous chitin synthase IIIa (CHSIIIa - Bcin04g03120) was chosen. Chitin synthases are β-glycosyltransferases that are transported by SVs to the plasma membrane where they catalyze the production of chitin fibers, a polymer of N-acetylglucosamine residues that contributes to the structural integrity of the fungal cell wall (Gonçalves et al., 2016). The gene encoding the fluorescent protein eGFP was inserted by homologous recombination at the 3' end of the *BcCHSIIIa* gene to produce the chimeric CHSIIIa::eGFP protein. In parallel, a strain was constructed that produces a cytoplasmic eGFP ($eGFP^{Cyt}$) under the control of the constitutive pOliC promoter.

Following growth on a glass surface, confocal microscopy was performed on both strains (Fig. 1A). The $eGFP^{Cyt}$ strain displayed a diffuse cytosolic fluorescent signal. In contrast, mobile fluorescent speckles and a stronger fluorescent signal concentrated at the apex could be observed in the CHSIIIa::eGFP strain. These last observations being consistent with previously reported localizations of SVs transporting chitin synthases (Wernet et al., 2023; Fukuda et al., 2009; Sánchez-León et al., 2011; Zhou et al., 2018), they validated the CHSIIIa::eGFP strain as a correct reporter strain.

Noticeably, the high apical fluorescence signal in the CHSIIIa::eGFP strain appeared either spheroid- or crescent-shaped (Fig. 1A). The spheroid shape was compatible with previous descriptions of the Spk (Khöli et al., 2008; Riquelme et al., 2014) and will be named as such hereafter. To our knowledge the crescent shape has not been reported in ascomycetes to describe the assembly of SVs at the tip of hyphae. To rule out the possibility of an artifact, 10 min time-lapse acquisitions were collected on 13 individual CHSIIIa::eGFP hyphae. For each acquisition, the apex was tracked, cropped and then a time-projection was performed to obtain a single image on which the geometry of the region of maximal fluorescence intensity could be measured. This geometry was that of a sphere (roundness > 0.5) in 7 hyphae out of 13 and that of a crescent

223 (roundness < 0.5) in the remaining 6 hyphae (Fig. 1C). Two populations of hyphae could therefore
224 be distinguished and those will be named « Spk-hyphae" and "crescent-hyphae" hereafter.

225 When the Spk- and crescent-hyphae were compared, no statistical difference was found in
226 hyphal width (3.237 ± 0.966 µm for crescent; 2.661 ± 0.414 µm for Spk, Student t-test, p-value
227 0.214) or in the apex curvature (1.304 ± 0.322 μm^{-1} for crescent; 1.665 ± 0.299 μm^{-1} for Spk,
228 Student t-test, p-value 0.08). No significant difference was observed either in the area of
229 maximum fluorescence intensity (0.424 ± 0.025 μm^2 for crescent; 0.431 ± 0.009 μm^2 for Spk;
230 Mann Whitney U-test, p-value 0.709).

231 **The Spk- and crescent-hyphae show different fluorescence variations**

232 For the 6 crescent-hyphae and the 7 Spk-hyphae, the recorded time-lapse acquisitions were used
233 to construct kymographs (signal along the growing axis of the apex over time; Fig. 2A & S1). As a
234 control, 5 hyphae of the $eGFP^{Cyt}$ strain were analyzed in parallel. In both the crescent- and Spk-
235 hyphae, these kymographs showed a more intense signal remaining concentrated at the apex over
236 time. By using the slope of the kymographs as an estimated value of the hyphal growth speed, no
237 significant difference could be observed between the average elongation rates of the hyphae
238 displaying a fluorescent Spk (378 ± 194 $nm.min^{-1}$) or crescent (211 ± 73 $nm.min^{-1}$) (Student t-test,
239 p-value 0.095).

240 The kymographs revealed hotspots of fluorescence intensity at the apex of the hyphae of the
241 CHSIIIa::eGFP strain (Fig. 2A & S1), indicating strong increase in fluorescence intensity in both
242 space (local accumulation of signal at the apex) and time (increase in fluorescence for a short
243 period of time). Considering that the fluorescence of eGFP could vary during time-lapse
244 acquisitions, due to the processes of folding and maturation of the protein, as well as to its
245 stability over time, these hotspots of fluorescence intensity could be linked to intrinsic behavior
246 of eGFP. To test this, the signals captured during time-lapse acquisitions of the $eGFP^{Cyt}$ and
247 CHSIIIa::eGFP strains were analyzed using Temporal Dynamics Clustering (TDC). The mean
248 fluorescence of the apical region (4 µm) of each individual hypha was measured at each time
249 point of the acquisitions in order to produce time series of fluorescence intensity. The first-order
250 difference was then computed for all time series and expressed as a cumulative first-order
251 difference (Fig. 2C). The TDC parameters u and I_q were calculated and used to partition each
252 individual cumulative distribution into the *main* and *tail* sections that distinguish common
253 variations from extreme events (see Methods). For each cumulative distribution, the mean value
254 of the *main* section (μ_{main}), its associated standard deviation (σ_{main}), and the mean value of the *tail*
255 section (μ_{tail}) were calculated. These coordinates were used for Fuzzy C-means clustering and this

identified two clusters, named cluster 1 and cluster 2, with a silhouette score of 0.761 (Fig. 2D). The difference in fluorescence variation in the hyphae that grouped in cluster 1 and 2 was supported by statistical differences in all 3 TDC parameters (Student t-test): μ_{main} (p-value 6.697e-9), σ_{main} (p-value 2.711e-9) and μ_{tail} (p-value 7.712e-9). The significant difference observed for metrics in the *main* section reveals that fluorescence variations do not differ between clusters solely on extreme events (*tail* section), but on their overall behavior. On the other hand, the medians of the overall fluorescence signals in the hyphae grouped in cluster 1 and 2 were not significantly different (Welch test, p-value 0.603). This indicated that cluster 2 did not differ from cluster 1 because of difference in fluorescence intensity inside the hyphae, but because of variations in fluorescence intensity over time.

Noticeably, cluster 1 grouped together the 5 hyphae of the $eGFP^{Cyt}$ strain and the 6 crescent-hyphae of the CHSIIIa::eGFP strain while cluster 2 grouped the 7 Spk-hyphae. In the 6 crescent-hyphae the variation in fluorescence at the apex could therefore not be distinguished from the one monitored in the $eGFP^{Cyt}$ strain, and it could therefore not be considered independent of the variations linked to the intrinsic behavior of eGFP. In contrast, the variation of fluorescence in the Spk-hyphae was stronger and independent of the intrinsic variations of eGFP (Fig. 2E).

Fluorescence variations are periodic in the Spk-hyphae

The results of the previous section showed that the 7 Spk-hyphae exhibited a fluorescent signal at the apex that strongly varied over time. A closer inspection of the signals of mean fluorescence intensity over time revealed an oscillation pattern (Fig. 2E & 3A). To explore this pattern, the Fast Fourier Transform (FFT) was applied and its output was expressed as amplitudes to obtain amplitude spectra (see Methods). In the specific example depicted in figure 3, the amplitude spectrum enabled the identification of a prominent oscillator at 39.75 seconds (Fig. 3B). When this period was used to produce a sinusoidal model, this model aligned correctly to the motifs observed on the kymograph (Fig. 3C). In all the Spk-hyphae, similar results were obtained (Fig. S2) and in all acquisitions the mean fluorescence intensity oscillated over time with one prominent oscillator identified with a period of 31 to 65 seconds (average 45.5 ± 10.1 seconds).

Considering that the observed oscillations could result from the displacement of the fluorescent CHSIIIa::eGFP particles along the z-axis of the hypha, cross-correlation was performed on the mean fluorescence intensity signals collected in 4 z-positions. Similar fluorescence variations within individual planes were validated by the obtained cross-correlation scores (Fig. S3). Under our conditions, the variations of fluorescence at the apex of the hyphae were therefore independent of movements of the CHSIIIa::eGFP in the z-dimension.

289 **Stepwise apical elongation in Spk- and crescent-hyphae**

290 Since CHSIIIa::eGFP is transported by SVs, the periodic variation of fluorescence intensity at the
291 apex of the Spk-hyphae could be due to successive increases and decreases in vesicles
292 accumulation at this location. SVs being supplied by the secretory pathway and destined to
293 exocytosis at the apex, such rhythmicity could be linked to periodic events of exocytosis. This
294 would result in discontinuous lipid additions to the plasma membrane and a stepwise pattern of
295 hyphal elongation. In contrast, the absence of significant variations in fluorescence intensity at
296 the apex of the crescent-hyphae over time could suggest constant SVs accumulation at this site
297 and thus the absence of periodic events of exocytosis. To explore this, an image analysis tool was
298 developed to first outline the apical region at each 4-sec time point of the time-lapse acquisitions,
299 and then to measure the distance travelled by the outline between frames to approximate the
300 dynamic of apical elongation (see Methods). As shown in figure 4, successive episodes of fast and
301 halted elongations were detected, producing a discontinuous hyphal expansion over time, but
302 they were detected in both some Spk- and crescent-hyphae. In some other hyphae of both types,
303 the pattern was less pronounced (Fig. 4, right) or mixed (Fig. S4). Within the limits of our
304 experimental conditions (resolution 130 nm/pixel, 4.455 sec/frame), both Spk- and crescent-
305 hyphae therefore exhibited large or small discontinuity in their apical elongation.

306

307 **Discussion**

308 Polar elongation in filamentous fungi relies on the restricted supply of secretory vesicles (SVs) to
309 the apex of growing hyphae. This represents a sequential process that includes the production of
310 these SVs by the Golgi apparatus, their transport at the apex, and finally their tethering and fusion
311 to the apical plasma membrane. In ascomycetes, the presence of a spitzenkörper (Spk) at the
312 apex reveals the spatially defined accumulation of SVs at this location before their tethering and
313 fusion mediated by the exocyst. In a contribution to the understanding of SV dynamics at the tip
314 of fungal hyphae, and to explore this aspect of fungal biology in a plant pathogenic fungus, the
315 class III chitin synthase BcCHSIIIa was fused to the fluorescent protein eGFP in *B. cinerea* and 10-
316 min time-lapse confocal microscopy recordings were carried out on living cells.

317 Chitin synthases are known cargoes of SVs and BcCHSIIIa plays an important role in the
318 development of *B. cinerea* (Soulié et al., 2006). Our results show that BcCHSIIIa::eGFP
319 accumulates at hyphal tips as in the ascomycetes *N. crassa* and *A. nidulans* (Fukuda et al. 2009;
320 Sánchez-León et al., 2011; Zhou et al., 2018). Our time-lapse recordings also showed a spheroid-
321 shaped fluorescent signal underneath the apical dome in half the analyzed hyphae. This validates

322 in living cells the once reported existence of a Spk in *B. cinerea*, on fixed cells, using electron
323 microscopy (Roberson et al., 2010). More unexpectedly, in the other half of the analyzed hyphae,
324 our recordings document an alternative organization of the SVs at the apex, in the shape of a
325 crescent. This is reminiscent of the observation of the *A. nidulans* CHSIIIa at the Spk and in an
326 apical crescent (Fukuda et al. 2009). It is also reminiscent of the apical vesicle crescent (AVC)
327 observed in mucoromycetous fungi (Grove and Bracker, 1970; Fisher and Robertson, 2016). It is
328 lastly reminiscent of the apical crescent formed by the exocyst in hyphae of *C. albicans* (Jones et
329 al. 2010) or *N. crassa* (Riquelme et al. 2014). A crescent-shape localization of SVs could therefore
330 correspond to their interaction with components of the exocyst. Interestingly, in *N. crassa,* some
331 exocyst components highlight a crescent whine another (Exo70) highlights the Spk (Riquelme et
332 al. 2014). And in *A. gossypii* some of these components highlight either a crescent or the Spk at
333 the tip of slow- and fast-growing hyphae, respectively (Köhli et al., 2008). This last observation led
334 to the hypothesis that a structural re-organization of the exocyst at the apex could be linked to the
335 rate of hyphal elongation (Köhli et al., 2008). The formation of a Spk would associate with fast
336 growing hyphae in *A. gossypii*, and this is supported by the observation of the Spk in mature fast
337 growing hyphae of *N. crassa*, and not in slower-growing germlings (Araujo-Palomares et al., 2007).
338 Remarkably, in the 13 hyphae analyzed in this study, the 4 fastest hyphae (≥ 399 $nm.min^{-1}$)
339 displayed a Spk while the two slowest hyphae (<155 $nm.min^{-1}$) displayed an apical crescent. The
340 remaining 7 hyphae, with elongation between 155 and 399 $nm.min^{-1}$, displayed either a Spk or a
341 crescent. This suggests that the Spk would associate with hyphal growth beyond a given threshold
342 (between 304 and 399 $nm.min^{-1}$ in *B. cinerea*). Below that threshold a Spk or a SVs crescent could
343 support similar elongation rates, exemplified by the Spk-hyphae of *N. crassa* elongating at 0.248
344 $\mu m.s^{-1}$ ± 0.00113 and the crescent-hyphae of *G. persicaria* elongating at 0.201 µm/s ± 0.00071.

345 By monitoring fluorescence levels at the apex over time, we also observed statistically different
346 behaviors between hyphae displaying a Spk or an apical crescent. The signals were analyzed
347 using TDC, a features-based clustering algorithm that can group signals based on their variability,
348 and this revealed the existence of two fluorescence behaviors. One of them was specific of
349 hyphae displaying a Spk and analysis of their signals through the Discrete Fourier Transform (DFT)
350 showed an oscillation with a period of 45.5±10.1 seconds. In a work published by Takeshita *et*
351 *al.* (2017), periodic oscillations of fluorescent chitin synthase at the apex of Spk-hyphae of
352 *N. crassa* and *A. nidulans* were also documented. A possible link between periodicity and tip
353 elongation was also noted by the authors, with *N. crassa* growing faster than *A.* nidulans and
354 exhibiting a shorter oscillation period (17 ± 6 seconds versus 30 ± 7 seconds). This link is
355 reinforced by our results since, under our conditions, *B. cinerea* hyphal elongation was slower

356 than that of *N. crassa* and *A. nidulans* and the measured periodicity was longer (45.5 ± 10
357 seconds). A faster periodicity in SVs supply could be necessary to sustain faster hyphal
358 elongation.

359 In the model proposed by Takeshita *et al*. (2017), a periodic release of SVs from the Spk would
360 induce a stepwise elongation of the plasma membrane through periodic waves of SVs exocytosis
361 at the apex. While required for polarized growth, spatially restricted exocytosis would however
362 induce the diffusion of lipid-bound polarity regulators that are also required for such growth
363 (Savage et al., 2012). Periodic exocytosis could allow for re-establishment of polarity between
364 waves (Takeshita, 2018; Wu et al., 2013). Through the tracking of the cell membrane in our
365 confocal time-lapse acquisitions, hyphae were identified that elongated in a discontinuous
366 manner, suggesting that waves of exocytosis could also occur in *B. cinerea*. Hyphae displaying a
367 more continuous elongation pattern, or a mixed pattern, were also identified, notably in the fast-
368 growing hyphae. This could result from short successive waves of exocytosis not detectable under
369 our conditions. Lastly, discontinuous elongation was found in hyphae displaying a Spk, but also
370 in hyphae displaying apical crescents with no detectable oscillation in fluorescence intensity.
371 Together with a discontinuous elongation also reported in hyphae displaying an AVC (López-
372 Franco et al. 1994), this calls for further investigation of the dynamics of SVs accumulation at the
373 apex and hyphal elongation.

374 In conclusion, this work on the ascomycetous plant pathogen *B. cinerea* documents the
375 coexistence, in the same environment, of two populations of hyphae. These population differ in
376 how SVs accumulate and behave at the apex. In one population SVs form a typical Spk and show
377 a periodic oscillation. In the other one, they accumulate in an apical crescent with no detectable
378 oscillation under our conditions.

379

References

Araujo-Palomares CL, Castro-Longoria E & Riquelme M (2007). Ontogeny of the Spitzenkörper in germlings of *Neurospora crassa*. Fungal Genet Biol. 2007 Jun;44(6):492-503. doi: 10.1016/j.fgb.2006.10.004.

Bartnicki-Garcia S, Hergert F & Gierz G (1989). Computer simulation of fungal morphogenesis and the mathematical basis for hyphal (tip) growth. Protoplasma 153, 46–57. https://doi.org/10.1007/BF01322464.

Bernardo SM, Rane HS, Chavez-Dozal A & Lee SA (2014). Secretion and filamentation are mediated by the *Candida albicans* t- SNAREs Sso2p and Sec9p. FEMS Yeast Res 14, 762–775. https://doi.org/10.1111/1567-1364.12165.

Boutillon A, Banavar SP & Campàs O (2024). Conserved physical mechanisms of cell and tissue elongation. Development. May 15;151(10):dev202687. doi: 10.1242/dev.202687.

Braun M & Richter P (1999). Relocalization of the calcium gradient and a dihydropyridine receptor is involved in upward bending by bulging of Chara protonemata, but not in downward bending by bowing of Chara rhizoids. Planta. Oct;209(4):414-23. doi: 10.1007/s004250050744.

Braun M, Hauslage J, Czogalla A & Limbach C (2004). Tip-localized actin polymerization and remodeling, reflected by the localization of ADF, profilin and villin, are fundamental for gravity-sensing and polar growth in characean rhizoids. Planta 219, 379–388. https://doi.org/10.1007/s00425-004-1235-4.

Braun M & Limbach C (2006). Rhizoids and protonemata of characean algae: model cells for research on polarized growth and plant gravity sensing. Protoplasma. Dec;229(2-4):133-42. doi: 10.1007/s00709-006-0208-9.

Cairns TC, Zheng X, Zheng P, Sun J & Meyer V (2021). Turning Inside Out: Filamentous Fungal Secretion and Its Applications in Biotechnology, Agriculture, and the Clinic. J Fungi (Basel) 7, 535. https://doi.org/10.3390/jof7070535.

Campanoni P & Blatt MR (2007). Membrane trafficking and polar growth in root hairs and pollen tubes. J. Exp. Bot. 58: 65–74.

Carol RJ & Dolan L (2002). Building a hair: tip growth in *Arabidopsis thaliana* root hairs. Philos. Trans. R. Soc. Lond. B Biol. Sci. 357, 815-821.https://doi.org/10.1098/rstb.2002.1092.

Cheung AY & Wu HM (2008). Structural and signaling networks for the polar cell growth machinery in pollen tubes. Annu. Rev. Plant Biol. 59: 547–572.

Crampin H, Finley K, Gerami-Nejad M, Court H, Gale C, Berman J & Sudbery P (2005). *Candida albicans* hyphae have a Spitzenkörper that is distinct from the polarisome found in yeast and pseudohyphae. J Cell Sci. Jul 1;118(Pt 13):2935-47. doi: 10.1242/jcs.02414.

Domozych DS, Fujimoto C & LaRue T (2013). Polar Expansion Dynamics in the Plant Kingdom: A Diverse and Multifunctional Journey on the Path to Pollen Tubes. Plants 2, 148– 173. https://doi.org/10.3390/plants2010148.

Fisher KE & Roberson RW (2016). Fungal Hyphal Growth – Spitzenkörper versus Apical Vesicle Crescent. Fungal Genom Biol, 6:1. DOI: 10.4172/2165-8056.1000136.

Fukuda K, Yamada K, Deoka K, Yamashita S, Ohta A & Horiuchi H (2009). Class III Chitin Synthase ChsB of *Aspergillus nidulans* Localizes at the Sites of Polarized Cell Wall Synthesis and Is

Required for Conidial Development. Eukaryot Cell 8, 945–956. https://doi.org/10.1128/EC.00326-08.

Geitmann A (2010). How to shape a cylinder: pollen tube as a model system for the generation of complex cellular geometry. Sex. Plant Reprod.23, 63-71. https://doi.org/10.1007/s00497-009-0121-4.

Gierz G & Bartnicki-garcia S (2001). A Three-Dimensional Model of Fungal Morphogenesis Based on the Vesicle Supply Center Concept. Journal of Theoretical Biology 208, 151–164. https://doi.org/10.1006/jtbi.2000.2209.

Gonçalves IR, Brouillet S, Soulié MC, Gribaldo S, Sirven C, Charron N, Boccara M & Choquer M (2016). Genome-wide analyses of chitin synthases identify horizontal gene transfers towards bacteria and allow a robust and unifying classification into fungi. BMC Evol Biol. Nov 24;16(1):252. doi: 10.1186/s12862-016-0815-9.

Grove SN & Bracker CE (1970). Protoplasmic Organization of Hyphal Tips Among Fungi: Vesicles and Spitzenkörper. J Bacteriol 104, 989–1009.

Haduch-Sendecka A, Pietruszka M & Zajdel P (2014). Power spectrum, growth velocities and cross-correlations of longitudinal and transverse oscillations of individual *Nicotiana tabacum* pollen tube. *Planta* **240**, 263–276.

Harris SD, Read ND, Roberson RW, Shaw B, Seiler S, Plamann M & Momany M (2005). Polarisome meets spitzenkörper: microscopy, genetics, and genomics converge. Eukaryot Cell. Feb;4(2):225-9. doi: 10.1128/EC.4.2.225-229.2005.

Hayakawa Y, Ishikawa E, Shoji J, Nakano H & Kitamoto K (2011). Septum-directed secretion in the filamentous fungus *Aspergillus oryzae*. *Molecular Microbiology* **81**, 40–55.

Ishitsuka Y, Savage N, Li Y, Bergs A, Grün N, Kohler D, Donnelly R, Nienhaus GU, Fischer R & Takeshita N (2015). Superresolution microscopy reveals a dynamic picture of cell polarity maintenance during directional growth. Sci Adv 1, e1500947. https://doi.org/10.1126/sciadv.1500947.

Jadhav R, Mach RL & Mach-Aigner AR (2024). Protein secretion and associated stress in industrially employed filamentous fungi. Appl Microbiol Biotechnol. Dec;108(1):92. doi: 10.1007/s00253-023-12985-4.

Jones LA & Sudbery PE (2010). Spitzenkorper, exocyst, and polarisome components in *Candida albicans* hyphae show different patterns of localization and have distinct dynamic properties. Eukaryot Cell 9, 1455–1465. https://doi.org/10.1128/EC.00109- 10.

Köhli M, Galati V, Boudier K, Roberson RW & Philippsen P (2008). Growth-speed-correlated localization of exocyst and polarisome components in growth zones of *Ashbya gossypii* hyphal tips. *J Cell Sci* **121**, 3878–3889.

Leroch M, Mernke D, Koppenhoefer D, Schneider P, Mosbach A, Doehlemann G, & Hahn M (2011). Living Colors in the Gray Mold Pathogen *Botrytis cinerea*: Codon-Optimized Genes Encoding Green Fluorescent Protein and mCherry, Which Exhibit Bright Fluorescence. Applied and Environmental Microbiology 77, 2887–2897. https://doi.org/10.1128/AEM.02644-10.

Li S, Francini G & Magli E (2023). Temporal dynamics clustering for analyzing cell behavior in mobile networks. *Computer Networks* **223**, 109578.

Lipowczan M & Pietruszka M (2017). Frequency-associated transition from single-cell asynchronous motion to monotonic growth. *J Biol Phys* **43**, 461–470.

López-Franco R, Bartnicki-Garcia S & Bracker CE (1994). Pulsed growth of fungal hyphal tips. Proc Natl Acad Sci U S A. Dec 6;91(25):12228-32. doi: 10.1073/pnas.91.25.12228.

Löpez-Franco R & Bracker CE (1996). Diversity and dynamics of the Spitzenkörper in growing hyphal tips of higher fungi. Protoplasma 195, 90–111. https://doi.org/10.1007/BF01279189.

Mullins ED, Chen X, Romaine P, Raina R, Geiser DM & Kang S (2001). *Agrobacterium*-Mediated Transformation of *Fusarium oxysporum*: An Efficient Tool for Insertional Mutagenesis and Gene Transfer. Phytopathology 91, 173–180. https://doi.org/10.1094/PHYTO.2001.91.2.173.

Riquelme M (2013). Tip growth in filamentous fungi: a road trip to the apex. Annu Rev Microbiol. 2013;67:587-609. doi: 10.1146/annurev-micro-092412-155652. Epub 2013 Jun 28.

Riquelme M, Bredeweg EL, Callejas-Negrete O, Roberson RW, Ludwig S, Beltrán-Aguilar A, Seiler S, Novick P & Freitag M (2014). The *Neurospora crassa* exocyst complex tethers Spitzenkörper vesicles to the apical plasma membrane during polarized growth. Mol Biol Cell 25, 1312–1326. https://doi.org/10.1091/mbc.E13-06-0299.

Riquelme M & Sánchez-León E (2014). The Spitzenkörper: a choreographer of fungal growth and morphogenesis. Curr Opin Microbiol 20, 27–33. https://doi.org/10.1016/j.mib.2014.04.003.

Roberson RW, Abril M, Blackwell M, Letcher P, McLaughlin DJ, Mouriño-Pérez R, Riquelme M & Uchida M (2010). Hyphal structure, in cellular and molecular biology of filamentous fungi. Cellular and Molecular Biology of Filamentous Fungi, 8–24.

Rolland S, Jobic C, Fèvre M, Bruel C (2003). *Agrobacterium*-mediated transformation of *Botrytis cinerea*, simple purification of monokaryotic transformants and rapid conidia-based identification of the transfer-DNA host genomic DNA flanking sequences. Curr Genet. Nov;44(3):164-71. doi: 10.1007/s00294-003-0438-8.

Sánchez-León E, Verdín J, Freitag M, Roberson RW, Bartnicki-Garcia S & Riquelme M (2011). Traffic of Chitin Synthase 1 (CHS-1) to the Spitzenkörper and Developing Septa in Hyphae of *Neurospora crassa*: Actin Dependence and Evidence of Distinct Microvesicle Populations. Eukaryotic Cell 10, 683–695. https://doi.org/10.1128/EC.00280-10.

Singh R, Caseys C & Kliebenstein DJ (2024). Genetic and molecular landscapes of the generalist phytopathogen *Botrytis cinerea*. Mol Plant Pathol. Jan;25(1):e13404. doi: 10.1111/mpp.13404.

Souibgui E, Bruel C, Choquer M, de Vallée A, Dieryckx C, Dupuy, JW, Latorse M-P, Rascle C & Poussereau N (2021). Clathrin Is Important for Virulence Factors Delivery in the Necrotrophic Fungus *Botrytis cinerea*. Frontiers in Plant Science 12.

Soulié MC, Perino C, Piffeteau A, Choquer M, Malfatti P, Cimerman A, Kunz C, Boccara M, Vidal-Cros A (2006). *Botrytis cinerea* virulence is drastically reduced after disruption of chitin synthase class III gene (Bcchs3a). Cell Microbiol. Aug;8(8):1310-21. doi: 10.1111/j.1462-5822.2006.00711.x.

Steinberg, G. (2007). Tracks for traffic: microtubules in the plant pathogen *Ustilago maydis*. New Phytologist 174, 721–733. https://doi.org/10.1111/j.1469-8137.2007.02072.x.

Taheri-Talesh N, Horio T, Araujo-Bazán L, Dou X, Espeso EA, Peñalva MA, Osmani SA & Oakley BR (2008). The Tip Growth Apparatus of *Aspergillus nidulans*. MBoC 19, 1439–1449. https://doi.org/10.1091/mbc.e07-05-0464.

Takano T, Funahashi Y & Kaibuchi K (2019). Neuronal Polarity: Positive and Negative Feedback Signals. Front Cell Dev Biol. Apr 24;7:69. doi: 10.3389/fcell.2019.00069.

Takeshita N, Wernet V, Tsuizaki M, Grün N, Hoshi HO, Ohta A, Fischer R & Horiuchi H (2015). Transportation of *Aspergillus nidulans* Class III and V Chitin Synthases to the Hyphal Tips Depends on Conventional Kinesin. PLoS One. May 8;10(5):e0125937. doi: 10.1371/journal.pone.0125937.

Takeshita N, Evangelinos M, Zhou L, Serizawa T, Somera-Fajardo RA, Lu L, Takaya N, Nienhaus GU, Fischer R (2017). Pulses of Ca2+ coordinate actin assembly and exocytosis for stepwise cell extension. Proc Natl Acad Sci U S A. May 30;114(22):5701-5706. doi: 10.1073/pnas.1700204114.

Takeshita N (2018). Oscillatory fungal cell growth. Fungal Genet Biol. Jan;110:10-14. doi: 10.1016/j.fgb.2017.12.002.

Savage NS, Layton AT & Lew DJ (2012). Mechanistic mathematical model of polarity in yeast. Mol Biol Cell. May;23(10):1998-2013. doi: 10.1091/mbc.E11-10-0837.

Virag A & Harris SD (2006).The Spitzenkörper: a molecular perspective. Mycol Res. Jan;110(Pt 1):4-13. doi: 10.1016/j.mycres.2005.09.005.

Wernet V, Kriegler M, Kumpost V, Mikut R, Hilbert L & Fischer R (2023). Synchronization of oscillatory growth prepares fungal hyphae for fusion. eLife 12, e83310. https://doi.org/10.7554/eLife.83310.

Wu CF & Lew DJ (2013). Beyond symmetry-breaking: competition and negative feedback in GTPase regulation. Trends Cell Biol. Oct;23(10):476-83. doi: 10.1016/j.tcb.2013.05.003.

Xie Y & Miao Y (2021). Polarisome assembly mediates actin remodeling during polarized yeast and fungal growth. J Cell Sci. Jan 8;134(1):jcs247916. doi: 10.1242/jcs.247916.

Zhou L, Evangelinos M, Wernet V, Eckert AF, Ishitsuka Y, Fischer R, Nienhaus GU & Takeshita N (2018). Superresolution and pulse-chase imaging reveal the role of vesicle transport in polar growth of fungal cells. Sci Adv 4, e1701798. https://doi.org/10.1126/sciadv.1701798.

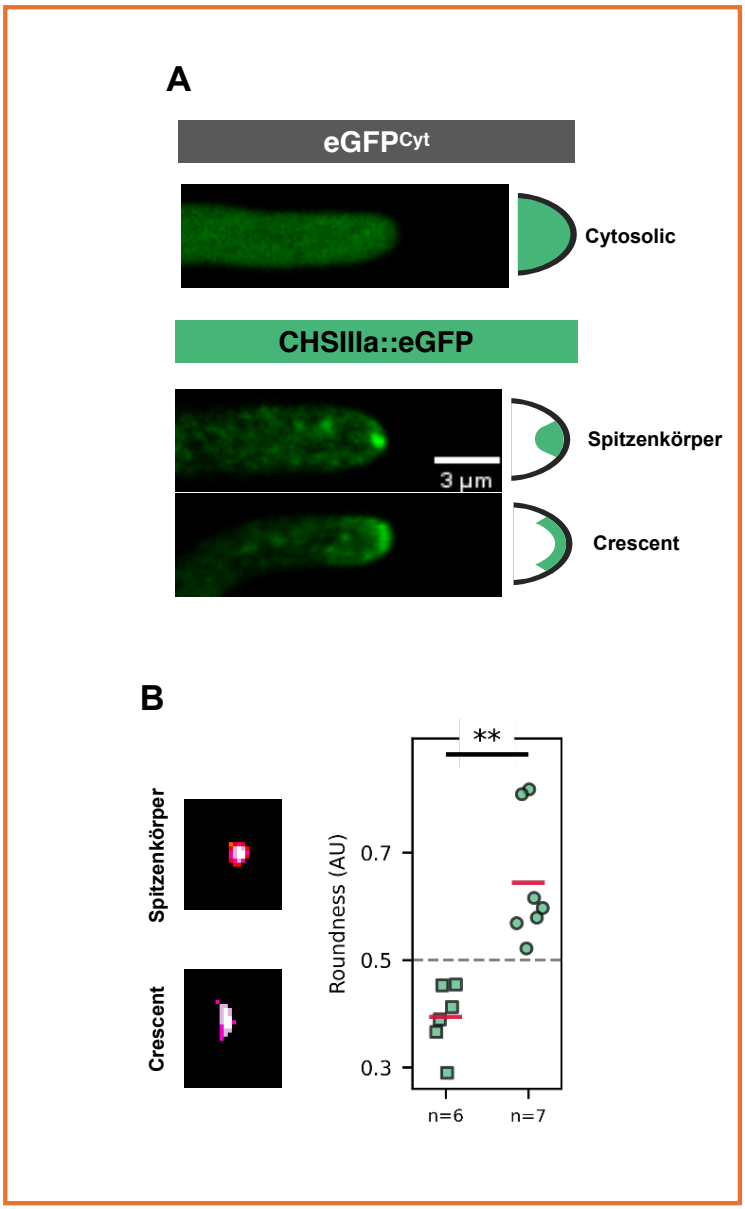

Fig.1 - Fluorescent chitin synthase CHSIIIa localizes at the apex of growing hyphae

A) Confocal image of the fluorescence signals at a growing apex of eGFP^{Cyt} and CHSIIIa::eGFP strains. Schemes on the right represent the homogenous distribution of the signal in the cytosol of the eGFP^{Cyt} hyphae and the two shapes of high intensity observed at the apices of the CHSIIIa::eGFP hyphae. B) Pseudo-colored images showing the shape of the regions of maximal fluorescence intensity at the apex of hyphae in the CHSIIIa::eGFP strain (Left), and measurement of the geometry of these regions (Right). Small red bar, median values. Mann-Whitney U test, p-value 0,001.

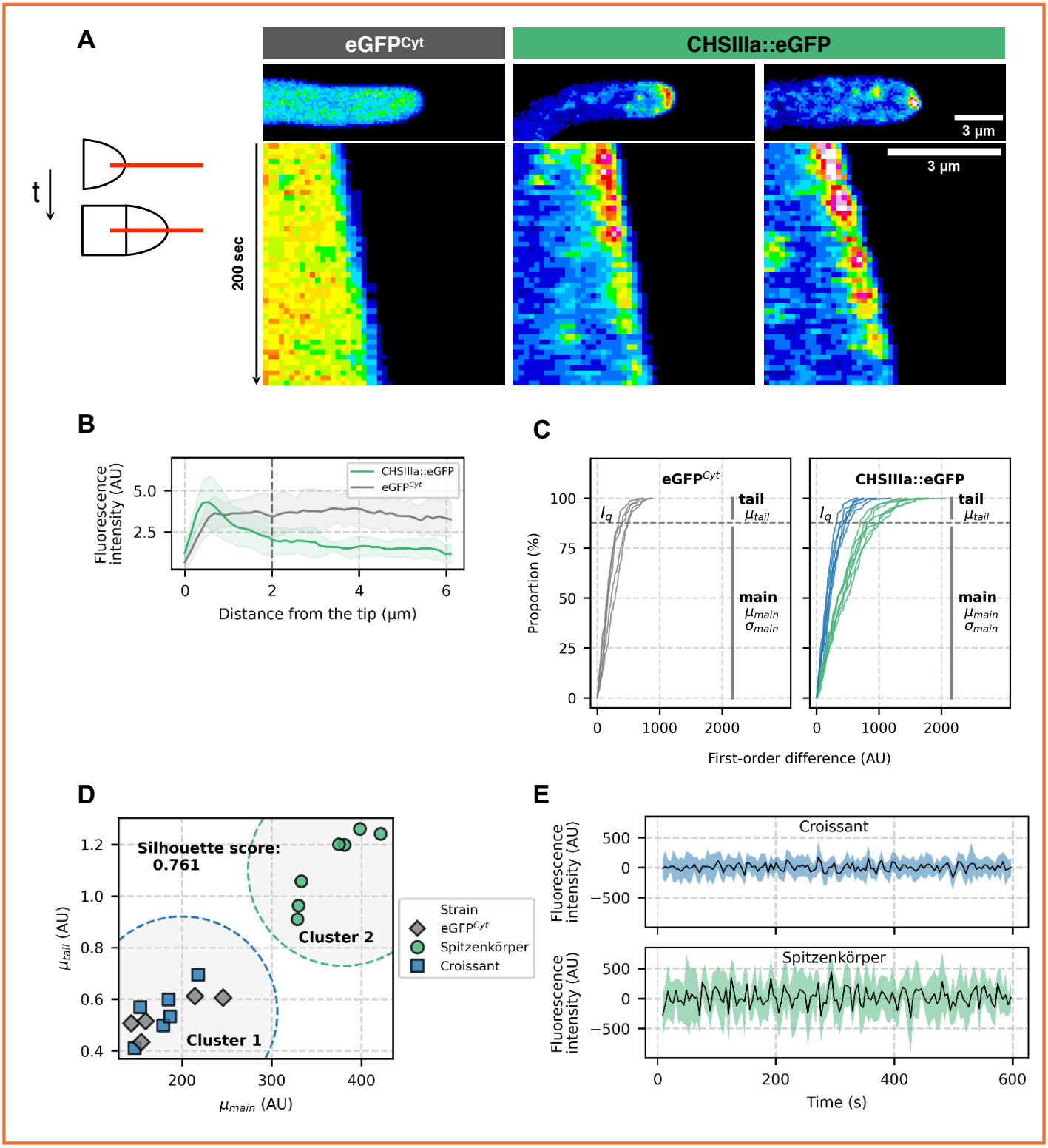

Fig.2 - Different fluorescence variations at the apex displaying a spitzenkörper (Spk) or a crescent. A) 16-colors LUT (blue to red: low to high fluorescent intensity) kymographs of eGFP^{Cyt} (left) and CHSIIIa::eGFP hyphae (right) along their growth axis (scheme on the left, red line). Total time 200 seconds. B) Measure of fluorescence intensity in the proximal (first 2 μm) and distal (2-6 μm) regions of the apex (n=5 for the eGFP^{Cyt} strain, n=13 for the CHSIIIa::eGFP strain). Solid lines, mean fluorescence intensity; pale colored areas, standard deviation. Comparison of fluorescence intensity between the proximal and 2-4 μm region did not reveal statistical difference in the eGFP^{Cyto} strain (Student t-test, p-value 0,359), but it did in the proximal region of the BcCHSIIIa::eGFP strain (Student t-test, p-value 0,001). C) Cumulative distribution of first-order signals obtained from time-lapse acquisitions (10 min) of 5 hyphae of the eGFP^{Cyt} strain (grey), 6 crescent-hyphae (blue) and 7 Spk-hyphae (green). The mean fluorescence was measured at each time point in the apical region (4.5±0.5 μm) of each hypha. Temporal Dynamics Clustering analysis generated the Iq parameter separating the main and tail sections characterized by their mean fluorescence intensities (μtail and μmain with its associated standard deviation (σmain)). D) Fuzzy C-means clustering using the μtail, μmain and σmain coordinates. E) Statistical analysis (Mann-Whitney U test, p-value 0.375) of fluorescence intensity measurements inside the eGFP^{Cyt}, Spk- and crescent-hyphae. Solid line: mean fluorescence; blue and green areas, standard deviation.

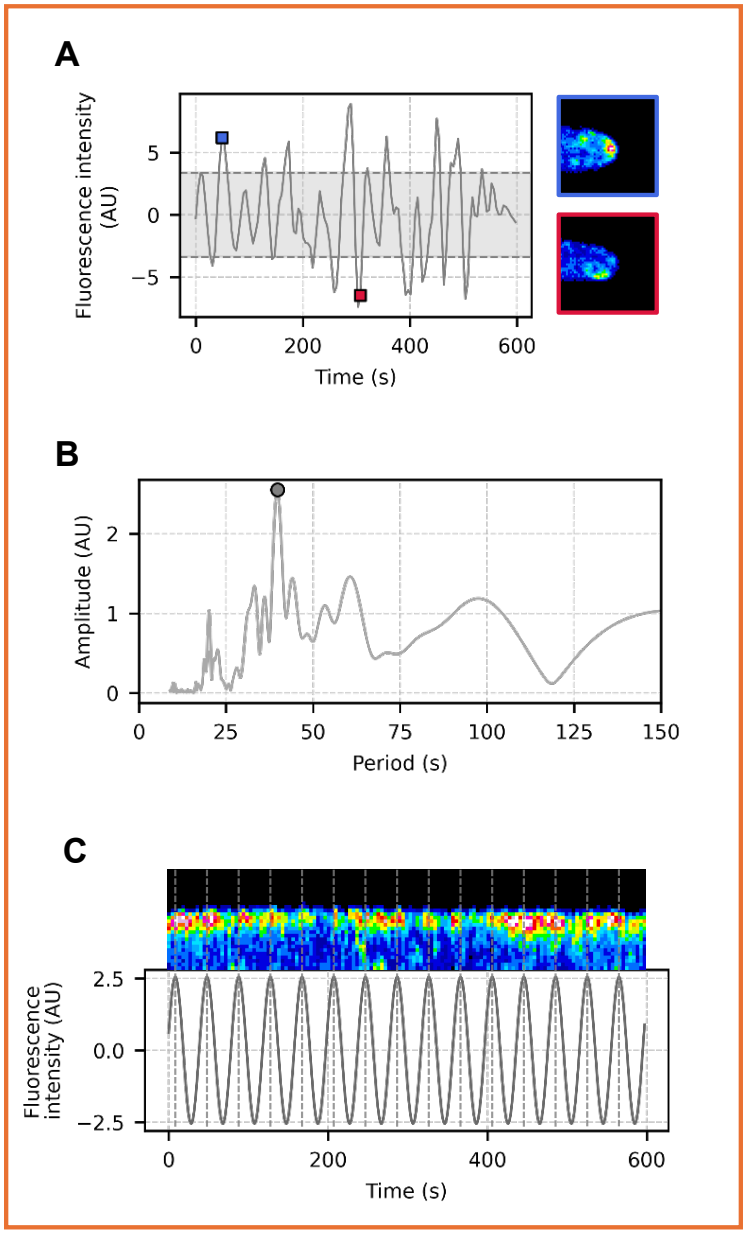

Fig.3. Periodic variations of the fluorescent signal at the apex of the Spk-hyphae.
A) Time evolution of the mean fluorescence intensity of the apical region (4.5±0.5 μm) of one Spk-hypha. Red and blue frames on the right, pseudo-colored images of the apex at times of high or low recorded fluorescent intensity (red and blue squares on the plot). Grey area, standard deviation of the signal. B) Fast Fourier Transform of the signal in A, expressed as an amplitude spectrum, and revealing a peak at 39 seconds (s) (grey dot) with an amplitude above the standard deviation (dashed line). C) Kymograph of the signal in A (top) aligned to a sinusoidal model built with a single 39 seconds period (bottom). See Fig. S2 for the other 6 Spk-hyphae analyzed.

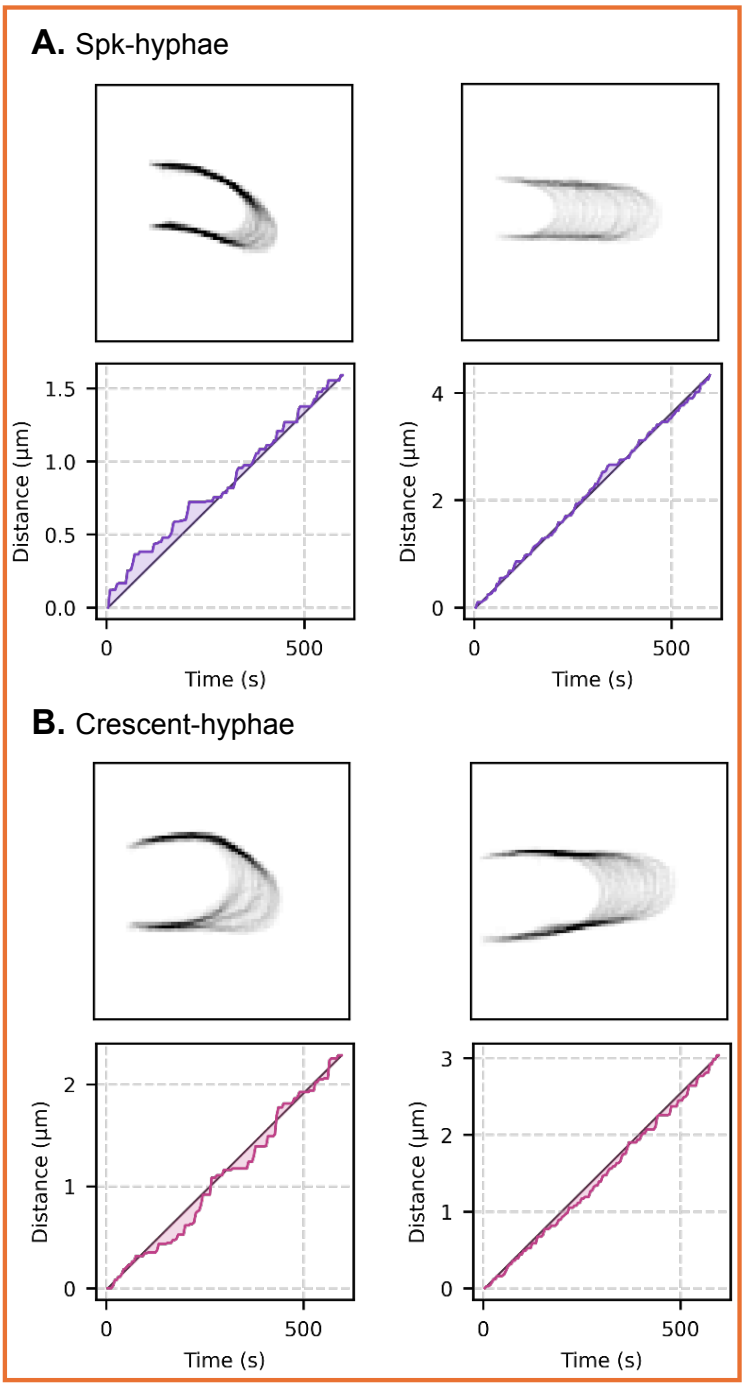

Fig.4 - Discontinuous hyphal elongation.
Ramp-and-stairs plots visualizing the distance travelled through time by different Spk- (A) and crescent-hyphae (B). Time projections (10 min, 4-sec steps) of cropped and outlined apices are shown on the top, with darker shades indicating periods of non-detectable growth. The corresponding hyphal elongations are plotted underneath, showing large and small stairs-like deviations from a theoretical continuous process (black diagonal).